Accepted Manuscript

Fractals

Article Title:	Fractal Analysis of Amphibole Aggregation Growth from a Basaltic Melt and Residual Melt at High Pressure and High Temperature
Author(s):	Xianxu Hu, Bo Zhang, Qizhe Tang, Jingui Xu, Dawei Fan, Wenge Zhou
DOI:	10.1142/S0218348X18500329
Received:	17 August 2017
Accepted:	24 November 2017
To be cited as:	Xianxu Hu *et al.*, Fractal Analysis of Amphibole Aggregation Growth from a Basaltic Melt and Residual Melt at High Pressure and High Temperature, *Fractals*, doi: 10.1142/S0218348X18500329
Link to final version:	https://doi.org/10.1142/S0218348X18500329

World Scientific
www.worldscientific.com

Accepted manuscript to appear in FRACTALS

Fractal Analysis of Amphibole Aggregation Growth from a Basaltic Melt and Residual Melt at High Pressure and High Temperature

XIANXU HU,*,† BO ZHANG,*,† QIZHE TANG,*,† JINGUI XU,* DAWEI FAN* and WENGE ZHOU*,‡

*Key Laboratory for High Temperature and High Pressure Study of the Earth's Interior

Institute of Geochemistry, Chinese Academy of Sciences

Guiyang 550081, P. R. China

†University of Chinese Academy of Sciences

Beijing 100049, P. R. China

‡zhouwenge@vip.gyig.ac.cn

Abstract

The aim of this work is to quantitatively explore the texture evolution of amphibole aggregation and residual melt with pressure and temperature. The amphibole aggregation growth from a basaltic melt and the residual melt at high pressure (0.6-2.6 GPa) and high temperature (860-970℃) exhibit statistical self-similarity which made us considering studying such characteristic by fractal analysis. The bi-phase box counting method was applied for fractal analysis of each product to identify the fractal phase and the fractal dimension was estimated. In the experimental products, the residual melt is identified as the fractal and amphibole as the Euclidean except for one experiment. The results show that the residual melt can be quantified by the fractal dimension(D_B) within the range of 1.782-1.848. The temperature has a significant effect on the morphology of

amphibole and the fractal dimension of the residual melt. The higher crystallization temperature is, the more regular amphibole grains are. At lower temperature (from 860℃to 915℃), the fractal dimension of the residual melt decreased with the increasing crystallization temperature, but at higher temperature (970℃), the fractal phase changed to amphibole and the fractal dimension of amphibole is 1.816. The pressure may be the dominant factor that controls the morphology of the mineral aggregation and the residual melt. The fractal dimension of melt decreased linearly with the increasing pressure and if the linear relationship between the fractal dimension and pressure can be further verified in the future, it can be used as a potential geological barometer.

Keywords: Fractals; Bi-Phase Box Counting; Amphibole; Residual Melt; High Temperature and High Pressure; Basaltic Melt.

1. INTRODUCTION

Since the concept of fractals was introduced by Mandelbrot (1967)[1] in terms of statistical self-similarity or scale invariance, many fields of scientific research have experienced the application of fractal geometry methods. The introduction of fractal geometry in Geosciences[2, 3] has also caused a growing interest in the use of fractal techniques to a large number of geological patterns and processes. Subsequently, many natural phenomena have been shown to exhibit statistical self-similarity. Examples include earthquakes, river networks, forest-fire, landslides, fragments, mineral deposits and porous media[3-9]. And many new techniques including ruler, box-counting, Cantor's Dust and area-perimeter methods have been developed to quantify geological features[3, 5, 7, 10-15]. Recently, an improved box-counting method called bi-phase box counting[16] has been developed to assist in identifying the most appropriate fractal model for describing binary images of natural fractal systems which provides an objective choose for fractal phases in binary images.

The fractal concepts have been widely used in many branches of geology and geophysics, however, relatively few applications in petrology[17-22]. Kruhl and Nega (1996)[17] applied ruler method to quartz boundaries and discovered that the shapes are dependent on the conditions of deformation with their complexity increasing with the decreasing temperature. Since then, several investigations about the fractal of quartz boundary have been reported[18, 19, 22]. In addition, Mamtani (2012)[20] applied area-perimeter method to fractal analysis of magnetite grains. Based on the fractal value of the magnetite shape, they

inferred that the shape of magnetite grains was not controlled by dislocation creep but the diffusion creep. Beside mentioned above, the comparative study of fractal analysis using different methods has also been carried out, for example, Volland and Kruhl (2004)[23] carried out the fractal analysis of a quartz-filled fracture zone by using the box-counting method and Cantor's Dust method.

Although the fractal analysis is not widely used in petrology, fractal geometry is really a powerful tool for quantifying complex patterns in the rock. The power of fractals in geology is that they have been proven to quantify, often by a single parameter (the fractal dimension, *D*), complex processes that would be otherwise difficult to quantify only by classic geological techniques[21]. At present, chemical and isotopic measurements[24, 25] dominate most part of current petrological studies, but the rock textures including the number, size, shape and spatial distribution of minerals should not be ignored because they reflect the relative kinetics of nucleation and growth which are in turn dependent on the geological process[26]. Among these factors, the mineral shape is usually the most difficult to quantify because of their irregular and complex form, but fractal geometry provides a simple and effective way to quantify the shape of mineral if the shape has a feature of self-similarity.

In this study, the fractal analysis was first applied to quantify the mineral aggregation and residual melt in the run products of melting-crystallization experiments at high pressure and high temperature. It was discovered that the shape of amphibole aggregation crystallizing from a basaltic melt at high pressure and high temperature has a feature of self-similarity, but according to the research of Perfect et al.[16], the real fractal phase is not

necessarily the amphibole. Hence, the bi-phase box counting method[16] was applied to identify the fractal phase (amphibole or melt) in the run product of melting-crystallization experiment. After that, the fractal dimension by box-counting method of the selected fractal phase was used for quantitative analysis of the texture evolution. The influence of pressure and temperature to the fractal dimension are discussed.

2. MATERIAL AND METHODS

2.1 Starting Material and Sample Assembly

The Starting material in our experiment is Cenozoic hydrous basalt. The basalt (Sample 10084) with a composition of plagioclase (40 wt.%), iddingsitized olivine (25 wt.%), clinopyroxene (20 wt.%), glass (10 wt.%) and minor iron titanium oxide (5 wt.%) sampled from the Yichuan – Ruyang region of western Henan province, central China. Table 1 shows the major elements and water content of the sample[27]. The basaltic rock contains 47.8 wt.% SiO_2 and 5.16 wt.% (Na_2O+K_2O). Using the TAS diagram[28], the basaltic rock can be classified as trachybasalt. The basaltic rock has a porphyritic texture. Phenocrysts are almost olivines (10 vol.%) which are iddingsitized along their rims and a small number of pyroxenes (<5 vol.%). The groundmass (85 vol.%) contains euhedral-subhedral plagioclase, clinopyroxene, iddingsitized olivine, and glass. The accessory minerals are ilmenite and apatite.

The experimental starting material was smashed and ground into a powder with particle size smaller than 15 μm. After that, the powder was taken into a muffle furnace for drying

to remove the adsorbed water at 200 ℃ for more than 10 hours. According to alphaMELTS[29], the liquidus of the basalt were estimated about 1150-1500℃ at 0.6 -2.6 GPa and the highest experimental temperatures (1460-1570℃ at 0.6-2.6 GPa) of our experiments were above the liquidus, which made certain that each sample of our experiments was completely melted.

The sample assembly consisted of a sintered pyrophyllite pressure medium, a cylindrical graphite heater and a graphite capsule (Fig. 1). The prepared sample powder was filled compactly to the graphite capsule to make sure that the cylindrical specimens were 4 mm in diameter and 3 mm in length before the experiments. Double-deck aluminium oxide tube was applied to insulate the graphite capsule from the graphite heater.

2.2 Experiments

The melting-crystallization experiments were performed in a multi-anvil pressure apparatus (JL-3600t), at the Key Laboratory for High Temperature and High Pressure Study of the Earth's Interior of the Institute of Geochemistry, Chinese Academy of Sciences, Guiyang, China. The pressure of the apparatus was calibrated by the melting curve of Au[30] and four other metals (Cu, Al, Pb and Zn)[31]. The uncertainty in pressure measurement is less than 0.05 GPa. Temperatures, measured and controlled automatically with $W_{95}Re_{05}$-$W_{74}Re_{26}$ thermocouples placed at the top of the graphite capsule, are considered accurate to ±5℃.

Two series of experiments were employed to reveal the influence of temperature and pressure to the fractal dimension of the amphibole aggregation and the residual melt.

(1) Isobaric sequence: Each run (Run 1, Run 2 or Run 3) was conducted at 0.6 GPa confining pressure. The temperature was rise to 1460℃ and maintained for one hour to make sure that the specimen was melted completely. After that, the temperature of each run was rapidly descended (< 1 min) to target (crystallization) temperature (860℃, 915℃, 970℃) and maintained for 100 hours.

(2) Isothermal sequence: Each run was conducted at different confining pressure and temperature (0.6 GPa and 1460℃, 1.1 GPa and 1490℃, 1.6 GPa and 1515℃, 2.1 GPa and 1540℃, 2.6 GPa and 1570℃) and maintained for one hour to make sure that the specimen was melted completely. After that, the temperature of each run was rapidly descended to 970℃ and maintained for 100 hours.

When each run was completed, the power of the multi-anvil pressure apparatus was cut off to quench the sample. Recovered samples were cut parallel to the axial direction of the cylindrical heater and then polished to thin sections. Chemical compositions of each experimental product were obtained using the JXA-8100 electron probe microanalyzer at the Institute of Geology and Geophysics, Chinese Academy of Sciences. A 15 Kv accelerating voltage and a 20 nA beam current were used for all analyses. Beam diameter was set to 1-5 μm and 10 μm for minerals and melts analysis, respectively. The backscatter electron (BSE) images of each experimental product were collected using the EPMA-1600 electron probe microanalyzer at the Institute of Geochemistry, Chinese Academy of Sciences. Operating conditions were similar to the former. The dimensions of the images are 2725×2367 pixels, and the pixel size is 0.22 μm for Run 1, Run 3 and 1.13 μm for Run 4 to Run 8 because of different magnifications (Fig. 3).

The chemical compositions of amphibole and residual melt of each run product was analyzed and the results are shown in Table 2. The volume percentage of amphibole in the experimental products is 35-58%, and the grain size of amphibole crystals is range from 5 μm in Run1 (0.6 GPa, 860℃, 100h) to 800 μm in Run 8 (2.6 GPa, 970℃, 100h). Amphibole is the main and stable crystalline phase in all the run products, although there is a very small amount of apatite, albite, spinel and magnetite. All of the amphibole grains in these experiments are calcic and the residual melts have granodioritic compositions (Table 2).

3 FRACTAL ANALYSIS OF EXPERIMENTAL GENERATED AMPHIBOLE AGGREGATION AND RESIDUAL MELT

3.1 The Box-counting Method

From the BSE images of amphibole grains and residual melt in each experimental product (Fig. 2-3), there seems to exist the self-similarity. Take the Run 1 for example (Fig. 2), when capturing partial enlarged views, it shows obvious similarity to primitive images. Therefore, the fractal analysis can be used to study the microstructure of amphibole grains and residual melt in our experimental products.

The classic definition of a self-similarity fractal is:

$$N = \frac{C}{r^{D}} \tag{1}$$

where N is the number of objects with a size r, C is a constant, and D is a fractal dimension[3, 32]. Equation (1) is linearized by log-log transformation, i.e.

$$\log(N) = \log(C) - D\log(r) \quad (2)$$

Practically, N is plotted against r on double logarithmic scale, and the graph is almost linear with slope -D. When relation (1) holds well, we can obtain the fractal dimensions D from the slop of the graph. This is the so-called box-counting method[33] which is a widely used method of fractal geometry due to its simplicity and capability.

In this study, the box-counting method is applied to get the fractal dimensions of amphibole aggregation and/or residual melt in each Run. A grid of square boxes of side length s is superimposed on the structure, which is on a line pattern. The numbers of non-empty boxes are counted. This procedure is repeated for as large a range of s-values as possible. Finally, the number $N(s)$ of the transected squares are plotted versus the side length s of the box in a double-logarithmic diagram. These data points exhibit a linear correlation if the investigated pattern is a fractal. The slope of this linear correlation represents the fractal 'box-counting' dimension D_B. In a plane, D_B can never exceed 2[34].

As we all know, gray-scale BSE images cannot be directly used to quantitatively analyze the microstructure until they are transformed to binary images. We therefore got the binary images firstly. The original 256-bit gray-scale BSE images were converted to binary using the Otsu's thresholding method[35]. Figure 3 (b) is an example of binary images thresholding from gray-scale BSE images of Run 8, and in the binary image any pixel is either black (melt) or white (amphibole). A designed program was used to count the pixels of amphibole or residual melt ($N(s)$) with different box size (s). In this work, all the images were cut into a square and the box size was set to be 1 pixel, 2 pixels, 3 pixels, …, to the largest pixels. The largest box size is usually smaller than half pixels of the image side

length, for example, if the square image with the size length is equal to M pixels, the largest box size is M/2 pixels or (M-1)/2 pixels. Figure 4 shows the plots of *log(N(s))* against *log(s)* obtained by the box-counting method. From each plot, the data show an excellent linear trend with the value of *log(s)* range from 0 to 2 equaling to the box size range from 1 pixel to 100 pixels which means there actually exists fractal features for the amphibole aggregation and/or residual melt in each run products. The points (box size smaller than 100 pixels) were chosen to generate a best-fit line by the least squares fitting and the negative slop of the best-fit line was the fractal dimension D_B.

3.2 Which Phase Is Fractal?

It is theoretically impossible for both phases in a binary image to be fractal[16]. For fractal systems of a binary image, if one phase is fractal, then the complement of counted fractal phase is Euclidean and should be scaled as:

$$N = \frac{C}{r^{E}} \tag{3}$$

Where E (=1, 2, or 3) is the Euclidean dimension. If the system is Euclidean, then both phases will scale according to Eq. (3). For this reason, the fractal phase (amphibole or residual melt) in our experiments should be identified firstly. The bi-phase box counting method advocated by Perfact and Donnelly[16] was used to distinguish which phase was fractal in the binary images.

In the case of bi-phase box counting, both phases are fitted conjointly using the following equations[16]:

$$\log(N_{Amp}) = \log(k_{Amp}) - D\log(s) \wedge \log(N_{Melt}) = \log(k_{Melt}) - 2\log(s) \quad (4a)$$

$$\log(N_{Melt}) = \log(k_{Melt}) - D\log(s) \wedge \log(N_{Amp}) = \log(k_{Amp}) - 2\log(s) \quad (4b)$$

$$\log(N_{Melt}) = \log(k_{Melt}) - 2\log(s) \wedge \log(N_{Amp}) = \log(k_{Amp}) - 2\log(s) \quad (4c)$$

Where ^ is the logical "AND" operator. Conjoint fitting means that both expressions are fitted to the box counting data simultaneously by minimizing the residuals using the method of least squares. In statistics, this process is known as segmented regression. The coefficient of determination (R^2) and residual sum of squares (RSS) are two important parameters used for judging which model (Eq. 4a, 4b or 4c) is most appropriate based on best fit statistics.

Here, we also took Run 1 for example (Fig. 4). According to Eq4, if the amphibole phase was selected as the fractal phase (D_B=1.936) and the residual melt phase should be Euclidean (E=2) (Fig.4a, fitting by Eq. 4a), then R^2=0.9948, RSS=0.679; if the residual melt phase was selected as the fractal phase (D_B=1.844) and the amphibole phase should be Euclidean (E=2) [Fig. 4b, fitting by Eq. (4b)], then R^2=0.9973, RSS=0.355; if both amphibole and melt phases are Euclidean (E=2), then R^2=0.9943, RSS=0.746. Based on the criteria of highest R^2 and/or lowest RSS values, the most appropriate model should be Eq. (4b) which means that the residual melt phase is fractal and the amphibole phase is Euclidean in Run 1. The results of the bi-phase box counting analyses of all Runs are summarized in Table 3. According to the results, the residual melt is the fractal phase for all Runs except Run 4. Moreover, our results show that the phase with smaller areal fractions is fractal in each Run which is agree with the results of Perfect and Donnelly (2015)[16].

3.3 The Influence of Different Field of View for The Fractal Analyses

Different field of view may affect the fractal dimension. In order to verify the consistency of the fractal dimension, five different randomly-selected fields of views (Part A, Part B, Part C, Part D and Part E) were analyzed using box-counting method to provide replication in each Run. Again, take Run 1 for example (Fig. 5), D_B of five different areas are 1.844 (± 0.012), 1.850 (±0.013), 1.853 (±0.013), 1.844 (±0.013), 1.850 (±0.014), respectively. The fractal dimension does not change significantly with the selected field of view used for the fractal analyses and the mean D_B is 1.848 (±0.004). Moreover, in all the experimental products, the fractal dimension shows the characteristic of consistency. Therefore, the mean value of the fractal dimension in each Run can be used as the estimated fractal dimension for the fractal phase. And the results of fractal analysis for the residual melt in all Runs are summarized in Table 4. Without regard to Run 4, the D_B values of the residual melt in our experimental products are within the range of 1.782-1.848 (Table 4) and the D_B value of the amphibole aggregation in Run 4 is 1.816. At different pressures and temperature conditions, the D_B values show some differences which may imply that the pressures and temperature have effects on the fractal dimension of the residual melt.

4. INFLUENCE OF PRESSURE AND TEMPERATURE ON TEXTURE EVOLUTION

4.1 Influence of Temperature

In the isobaric sequence (Fig. 3, Run 1, Run 3, Run 4), the morphology and particle size of amphibole grains vary significantly with temperature. In Run 1 (860℃), the amphibole

grains are dendritic and highly irregular. With increasing temperature, in Run 3 (915℃), the amphibole grains are subhedral-granular and the particle size is about 50 μm. In Run 4 (970℃), the amphibole grains are also subhedral-granular but the particle size increases to more than 60 μm. Overall, with the increase of temperature, the amphibole grains grow more regular and the size increases obviously. Our experiments in the isobaric sequence were conducted at the same pressure and initial melting temperature T_0 (1460℃), so the liquidus temperature $T_{liquidus}$ is equal to each other. The practically crystallization temperature T is the only variable factor for the amphibole crystallization. From Run1 to Run4, the degree of undercooling $\triangle T=T_{liquidus}-T$, gradually reduces and the integrality of amphibole increases (Fig. 3). The degree of undercooling can influence the morphology of crystals obviously. For example, Faure et al. [36] observed that the evolution of forsterite morphology is from tablets to hopper (skeletal) crystals, and then to swallowtail shapes (dendritic morphology) with increasing degree of undercooling. Our experiments show a similar trend for the evolution of amphibole morphology with increasing temperature.

As summarized in Table 3, the fractal phase is the residual melt in Run 1 and Run 3, and D_B is 1.844±0.012 and 1.780±0.005, respectively. However, in Run 4, the fractal phase is no longer the residual melt but the amphibole phase (D_B =1.816±0.008) which means that the residual melt in Run 4 is actually the Euclidean dimension and the dimension of the residual melt is equal to 2. The D_B of the residual melt in the isobaric sequence shows a complex behavior with increasing temperature (Fig. 4a). From Run 1 to Run 3, with increasing temperature, the fractal dimension of the residual melt reduced from 1.844 to

1.780, it seems that the temperature has an opposite effect on the fractal dimension of the residual melt. But when the temperature reached 970℃, the fractal phase changed that the residual melt become Euclidean and amphibole aggregation become fractal. The previous study of Perfect and Donnelly[16] indicated that the phase with the areal fraction(Φ) < 50% is the fractal phase. In our experiment, only in Run 4, the Φ of amphibole aggregation is smaller than 50% and the amphibole aggregation is the fractal phase which is consistent with the result of Perfect and Donnelly[16]. Hence, it seem that the Φ may be the reason for the sudden change. However, there is only one example at present study. Therefore, more detailed researches need to be done in the future for determining whether the sudden change of fractal phase is a particular case for Run 4 in our experiments or universal phenomenon.

4.2 Influence of Pressure

Since the experiments in the isothermal sequence were carried out at the same crystallization temperature (970℃), the run products of the isothermal sequence gave us a good opportunity to discuss the effects of pressure on the morphology of amphibole and fractal dimension of the residual melt.

In the isothermal sequence (Fig. 3, Run 4 to Run 8), the morphology and particle size of amphibole vary significantly with increasing pressure. In Run 4, the amphibole grains are subhedral-granular and the particle size is larger than 60 μm. In Run 5, the amphibole grains are subhedral and the particle size is nearly 100 μm. In Run 6, the amphibole morphology developed to euhedral (elongated grains) and the particle size is about 300

μm. In Run 7 and 8, the amphibole grains are more euhedral and the particle size increases gradually. In Run 8, the biggest amphibole grain is nearly 800 μm. Our experiments in the isothermal sequence were conducted at the same crystallization temperature (970℃). Using the software alphaMELTS[27], the liquidus of the basalt was estimated as: 1150℃/0.6 GPa (Run 4), 1175℃/1.1 GPa (Run 5), 1250℃/1.6 GPa (Run 6), 1400℃/2.1 GPa (Run 7), and 1500℃/2.6GPa (Run 8). While the practically crystallization temperature T is 970℃, the degree of undercooling ($\Delta T=T_{liquidus}-T$) at different pressures can be calculated as: 180℃ (0.6 GPa), 205℃ (1.1 GPa), 280℃ (1.6 GPa), 430℃ (2.1 GPa), 530℃ (2.6 GPa). As mentioned above, the degree of undercooling has an opposite effect on the morphology of crystals obviously. But in the isothermal sequence, the result is quite different. Because the degree of undercooling increases with pressure and the crystal integrality decreases gradually with the increasing degree of undercooling, the amphibole grains are more euhedral and the particle size increases gradually with increasing pressure may indicate that with respect to the degree of undercooling, the pressure is the most important factor affecting mineral morphology and particle size at the pressure range of our experiments in isothermal sequence.

As previously mentioned, the fractal phase is the residual melt in the whole isothermal sequence except Run 4, therefore, we only discuss the fractal dimension of the residual melts from Run 5 to 8 without regard to Run 4. The fractal dimensions of the residual melts from Run 5 to 8 were acquired by box-counting method and the results are: 1.846±0.003 (Run 5), 1.827±0.005 (Run 6), 1.803±0.003 (Run 7), 1.800±0.005 (Run 8) (Table 4). The relationship between the fractal dimensions of melt and pressure in each

Run in isothermal sequence is shown in Fig. 6b. The fractal dimensions D_B continuously decreases as a linear function of pressure. The linear regression equation is D_B=-0.0324(±0.0063)P+1.8789(±0.0121) (R^2=0.9306). The equation can also be transformed as:

$$P=-28.7(\pm5.5)D_B+54.1(\pm10.1) \quad (R^2=0.9306) \qquad (3)$$

where D_B is the fractal dimension by box-counting method and P is the pressure whose unit is GPa. This equation means that if the residual melt phase is fractal and the fractal dimension of the residual melt can be measured, the pressure can be estimated by the linear relationship between the pressure and fractal dimension value. Moreover, if this relationship is prevalent in natural rocks whose mineral aggregation or melt has fractal feature, it can be used as a potential geological barometer. Once we get the D_B value from the mineral aggregation or melt through the box-counting method, the practically crystallization pressure can be evaluated by a similar equation like Eq. (3). Furthermore, the equation is particularly useful for the estimation of pressure on natural rocks that cannot be settled by the traditional geological barometer. However, it needs to be reminded that this relationship still needs further experimental confirmation.

In summary, from the results of our experiments in the isothermal sequence, it can be speculated that the pressure may be the dominant factor for the morphology of mineral aggregation. The fractal dimension of the residual melt provides quantification analysis to the evolution of mineral and residual melt morphology. Furthermore, the linear relation between the fractal dimension and pressure may probably be used as a potential geological barometer.

5. CONCLUSIONS

Microstructure of amphibole aggregation growth from the hydra-basalt melt and residual melt at 0.6-2.6 GPa and 860-970℃ shows self-similarity, but which phase is the most appropriate fractal should be identified circumspectly. By using the bi-phase box counting method, the residual melt is identified as the fractal and amphibole as the Euclidean except for Run 4. Applying the box-counting method, the fractal dimension (D_B) of the residual melt within the range of 1.782-1.848 has been acquired. Pressure is the dominant factor for the fractal evolution at the same crystallization temperature. A linear relationship between the D_B value and pressure was obtained and if this relationship can be verified in the future, the P-D_B relationship can be used as a potential geological barometer. The influence of temperature on the amphibole growth is manifested by the crystal morphology and particle size. At lower temperature (from 860℃ to 915℃), the fractal phase was the residual melt and the D_B value of melt reduced with increasing temperature, but at higher temperature (970℃), the fractal phase suddenly changed to amphibole. It seems that the areal fraction (Φ) may be the reason for the sudden change. However, further detailed experimental studies on the crystallization of different minerals at high temperature and high pressure combined with the fractal analyses will provide much more precise constraints on the effects of the temperature and pressure on the fractal of minerals and melt.

ACKNOWLEDGMENTS

Research is supported by the Strategic Priority Research Program (B) of the Chinese Academy of Sciences (XDB 18010401), the Joint Research Fund in Huge Scientific Equipment (U1632112) under cooperative agreement between NSFC and CAS, the National Natural Science Foundation of China (Grant No. 41772043 and 41374107). And CAS"Light of West China" Program (2017, to Dawei Fan)

REFERENCES

1. B. B. Mandelbrot, How long is the coast of Britain? Statistical self-similarity and fractional dimension, *Science* **156** (3775) (1967) 636-638.

2. D. L. Turcotte, Fractals in Geology and Geophysics, *Pure Appl Geophys* **131** (1-2) (1989) 171-196.

3. D. L. Turcotte, *Fractals and Chaos in Geology and Geophysics*, 2 ed. (Cambridge University Press, 1997).

4. B. M. Yu, J. C. Cai and M. Q. Zou, On the physical properties of apparent two-phase fractal porous media, *Vadose Zone J* **8** (1) (2009) 177-186.

5. M. K. Sachs, M. R. Yoder, D. L. Turcotte, J. B. Rundle and B. D. Malamud, Black swans, power laws, and dragon-kings: Earthquakes, volcanic eruptions, landslides, wildfires, floods, and SOC models, *Eur Phys J-Spec Top* **205** (1) (2012) 167-182.

6. B. L. Cox and J. S. Y. Wang, Fractal Surfaces: Measurement and Applications in the Earth Sciences, *Fractals* **1** (1) (1993) 87-115.

7. J. P. Ortiz, R. C. Aguilera, A. S. Balankin, M. P. Ortiz, J. C. T. Rodriguez, M. A. A. Mosqueda, M. A. M. Cruz and W. Yu, Seismic Activity Seen through Evolution of the Hurst Exponent Model in 3d, *Fractals* **24** (4) (2016)

8. L. J. You, Q. Chen, Y. L. Kang, Y. F. Yu and J. G. He, Evaluation of formation damage using microstructure fractal in shale reservoirs, *Fractals* **23** (1) (2015)

9. Y. L. Zhang, Q. Sun, H. He, L. W. Cao, W. Q. Zhang and B. Wang, Pore characteristics and mechanical properties of sandstone under the influence of temperature, *Appl Therm Eng* **113** (2017) 537-543.

10. B. D. Malamud, G. Morein and D. L. Turcotte, Forest fires: An example of self-organized critical behavior, *Science* **281** (5384) (1998) 1840-1842.

11. B. D. Malamud and D. L. Turcotte, Self-affine time series: I. Generation and analyses, *Advances in Geophysics* **40** (1999) 1-90.

12. C. G. Sammis, R. H. Osborne, J. L. Anderson, M. Banerdt and P. White, Self-Similar Cataclasis in the Formation of Fault Gouge, *Pure Appl Geophys* **124** (1-2) (1986) 53-78.

13. D. L. Turcotte and B. D. Malamud, Landslides, forest fires, and earthquakes: examples of self-organized critical behavior, *Physica A* **340** (4) (2004) 580-589.

14. D. L. Turcotte, Self-organized complexity in geomorphology: Observations and models, *Geomorphology* **91** (3-4) (2007) 302-310.

15. F. P. Agterberg, Fractals and Spatial Statistics of Point Patterns, *J Earth Sci-China* **24** (1) (2013) 1-11.

16. E. Perfect and B. Donnelly, Bi-Phase Box Counting: An Improved Method for Fractal Analysis of Binary Images, *Fractals* **23** (1) (2015)

17. J. H. Kruhl and M. Nega, The fractal shape of sutured quartz grain boundaries: Application as a geothermometer, *Geol Rundsch* **85** (1) (1996) 38-43.

18. S. Majumder and M. A. Mamtani, Fractal analysis of quartz grain boundary sutures in a granite (Malanjkhand, Central India) - Implications to infer regional tectonics, *J Geol Soc India* **73** (3) (2009) 309-319.

19. M. A. Mamtani, Strain-rate Estimation Using Fractal Analysis of Quartz Grains in Naturally Deformed Rocks, *J Geol Soc India* **75** (1) (2010) 202-209.

20. M. A. Mamtani, Fractal analysis of magnetite grains - implications for interpreting deformation mechanism, *J Geol Soc India* **80** (3) (2012) 308-313.

21. D. Perugini and U. Kueppers, Fractal analysis of experimentally generated pyroclasts: A tool for volcanic hazard assessment, *Acta Geophys* **60** (3) (2012) 682-698.

22. M. Takahashi, Fractal analysis of experimentally, dynamically recrystallized quartz grains and its possible application as a strain rate meter, *J Struct Geol* **20** (2-3) (1998) 269-275.

23. S. Volland and J. H. Kruhl, Anisotropy quantification: the application of fractal geometry methods on tectonic fracture patterns of a Hercynian fault zone in NW Sardinia, *J Struct Geol* **26** (8) (2004) 1499-1510.

24. M. Wang, X. Zhang, et al., Zircon U–Pb dating of Pubei granite and strontium isotope from sphalerite of the Xinhua Pb–Zn–(Ag) deposit, Yunkai Area of Guangxi Province, South China, *Acta Geochimica* **35**(2) (2016) 156-171.

25. Meng, Z., Q. Zhang, et al., The genetic relationship between Habo alkaline intrusion and its surrounding deposits, Yunnan Province, China: geological and S–Pb isotopic evidences, *Acta Geochimica* **35**(4) (2016) 391-407.

26. M. D. Higgins, Verification of ideal semi-logarithmic, lognormal or fractal crystal size distributions from 2D datasets, *Journal of Volcanology and Geothermal Research* **154** (1-2) (2006) 8-16.

27. W. G. Zhou, B. R. Zhang, Z. D. Zhao and H. S. Xie, Geochemical characteristics and the provenance of cenozoic basic volcanic rocks in western Henan province, China, *Journal of Mineralogy and Petrology* (03) (1998) 52-58 (In Chinese with English abstract).

28. E. A. K. Middlemost, Naming materials in the magma igneous rock system, *Earth-Sci Rev* **37** (3-4) (1994) 215-224.

29. P. M. Smith and P. D. Asimow, Adiabat_1ph: A new public front-end to the MELTS, pMELTS, and pHMELTS models, *Geochem Geophy Geosy* **6** (2005)

30. H. F. Fu and C. M. Zhu, Testing parameters such as temperature, pressure in static super high pressure apparatus, *Physic* **9** (03) (1980) 193-195 (In Chinese with English abstract).

31. S. M. Shan, R. P. Wang, J. Guo and H. P. Li, Pressure calibration for the sample cell of YJ-3000t multi anvil press at high temperature and high pressure, *Chinese Journal of High Pressure Physics* **21** (04) (2007) 367-372 (In Chinese with English abstract).

32. D. L. Turcotte, Fractals in petrology, *Lithos* **65** (3-4) (2002) 261-271.

33. R. Lopes and N. Betrouni, Fractal and multifractal analysis: A review, *Med Image Anal* **13** (4) (2009) 634-649.

34. T. Hirata, Fractal Dimension of Fault Systems in Japan - Fractal Structure in Rock Fracture Geometry at Various Scales, *Pure Appl Geophys* **131** (1-2) (1989) 157-170.

35. N. Otsu, Threshold selection method from gray-level histograms, *IEEE T rans. Syst. Man. Cybern.***9** (1979) 62-66.

36. F. Faure, G. Trolliard, C. Nicollet and J. M. Montel, A developmental model of olivine morphology as a function of the cooling rate and the degree of undercooling, *Contrib Mineral Petr* **145** (2) (2003) 251-263.

Table 1 [a]Bulk Chemical Composition of the Experimental Starting Material (Sample 10084), wt%

[b]10084	SiO_2	TiO_2	Al_2O_3	FeO	Fe_2O_3	MnO	MgO	CaO	Na_2O	K_2O	P_2O_5	CO_2	H_2O+	total
wt%	47.80	2.48	14.13	3.53	7.57	0.16	6.44	8.40	3.90	1.26	0.90	0.02	3.33	99.92

[a] Data is from Zhou et al. 1998

[b] Sample No. 10084

Table2

Table 2 Major Element Analyses of Amphibole and Melt

	Run 1		Run 3		Run 4		Run 5		Run 6		Run 7		Run 8	
[a]Con-dition	0.6 GPa-860 ℃ -100h		0.6 GPa-915 ℃ -100h		0.6 GPa-970 ℃ -100h		1.1 GPa-970 ℃ -100h		1.6 GPa-970 ℃ -100h		2.1 GPa-970 ℃ -100h		2.6 G-970 ℃ -100h	
[b]Phase	Amp	Melt	Amp	Melt	Amp	Melt	Amp	Melt	Amp	Melt	Amp	Melt	Amp	Melt
O_2	41.35	60.30	40.51	61.73	39.54	58.66	40.24	58.27	39.41	62.11	40.63	59.08	38.69	60.90
Al_2O_3	13.59	21.75	14.06	19.31	13.48	18.40	14.47	19.25	15.40	18.08	16.42	18.18	15.89	19.07
TiO_2	3.43	0.11	3.57	0.48	5.16	0.81	3.80	0.76	3.88	0.71	2.95	0.73	3.37	0.82
Cr_2O_3	0.16	0.08	0.06	0.03	0.16	0.03	0.03	0.02	0.02	0.02	0.08	0.03	0.06	0.03
MgO	11.63	0.04	10.67	0.48	10.91	1.19	10.81	0.85	8.83	0.53	9.96	0.64	7.50	0.43
NiO	0.02	0.02	0.00	0.01	0.01	0.02	0.01	0.01	0.03	0.03	0.01	0.01	0.02	0.03
FeO*	13.57	0.63	13.39	3.09	13.96	6.92	13.19	4.75	14.76	3.34	12.23	3.15	12.78	2.76
MnO	0.19	0.04	0.20	0.07	0.18	0.11	0.18	0.13	0.17	0.06	0.16	0.08	0.17	0.06
CaO	10.00	6.32	11.08	2.62	10.30	4.05	10.77	3.07	9.78	2.02	9.64	2.35	10.71	2.00
Na_2O	2.72	7.11	2.83	6.58	2.82	5.08	2.80	5.80	3.03	5.10	3.07	5.75	3.36	4.61
K_2O	0.74	1.31	1.04	1.13	0.77	0.95	1.18	2.30	1.49	1.40	1.65	4.07	1.68	1.76
Total	97.38	97.71	97.41	95.51	97.29	96.24	97.47	95.20	96.81	93.41	96.79	94.06	94.21	92.46

[a] The experimental condition of each Run. For example, 0.6 GPa-860°C-100h means the pressure is 0.6 GPa, the crystallization temperature is 860℃, and the crystallization period is 100 hours.

[b] Abbreviations of phases: Amp=amphibole, Melt=residual melt

FeO*, total iron.

Table 3 Summary of Best Fit Parameters and Regression Statistics[a] from the Conjoint Fitting of Eq. (4) to Box Counting Results for the amphibole (Amp) and the residual melt Phases of Each Run.

Image	Assumed Fractal Phase (Φ)	log $k_{Amp}(S_E)$	log $k_{Melt}(SE)$	D/E(S_E)	R^2	RSS	Inferred Fractal Phase
Run1	Amp(64.7%)	5.429(0.009)	6.106(0.008)	1.936(0.006)	0.9948	0.679	
	Melt(35.3%)	5.531(0.003)	5.860(0.020)	1.844(0.012)	0.9973	0.355	Melt
	Neither	5.531(0.003)	6.106(0.008)	2.000(0.000)	0.9943	0.746	
Run3	Amp(57.8%)	5.937(0.005)	6.213(0.009)	1.856(0.003)	0.9921	0.837	
	Melt(42.2%)	6.164(0.006)	5.866(0.009)	1.780(0.005)	0.9963	0.391	Melt
	Neither	6.164(0.006)	6.213(0.009)	2.000(0.000)	0.9890	1.169	
Run4	Amp(42.6%)	5.725(0.012)	6.400(0.005)	1.816(0.008)	0.9970	0.350	Amp
	Melt(57.4%)	6.016(0.008)	6.219(0.009)	1.855(0.005)	0.9942	0.683	
	Neither	6.016(0.008)	6.400(0.005)	2.000(0.000)	0.9924	0.896	
Run5	Amp(56.4%)	6.023(0.009)	6.456(0.007)	1.894(0.005)	0.9953	0.543	
	Melt(43.6%)	6.191(0.005)	6.216(0.015)	1.848(0.009)	0.9970	0.353	Melt
	Neither	6.191(0.005)	6.456(0.007)	2.000(0.000)	0.9938	0.724	
Run6	Amp(60.7%)	5.890(0.008)	6.159(0.008)	1.897(0.005)	0.9941	0.662	
	Melt(39.3%)	6.052(0.005)	5.890(0.016)	1.829(0.010)	0.9968	0.363	Melt
	Neither	6.052(0.005)	6.159(0.008)	2.000(0.000)	0.9926	0.832	
Run7	Amp(65.4%)	5.836(0.006)	6.095(0.009)	1.907(0.004)	0.9921	0.877	
	Melt(34.6%)	5.982(0.004)	5.775(0.018)	1.798(0.011)	0.9968	0.357	Melt
	Neither	5.982(0.004)	6.095(0.009)	2.000(0.000)	0.9909	1.015	
Run8	Amp(65.4%)	6.104(0.004)	6.409(0.009)	1.893(0.002)	0.9921	0.869	
	Melt(34.6%)	6.274(0.004)	6.082(0.017)	1.793(0.011)	0.9967	0.368	Melt
	Neither	6.274(0.004)	6.409(0.009)	2.000(0.000)	0.9905	1.054	

[a] Φ=areal fractions of each phase, S_E= standard error, R^2=coefficient of determination, RSS= residual sum of squares.

Table 4 Parameter Setting of the Experiments and the Results of the Fractal Analysis for the residual melt in each Run.

	T/℃	P/GPa	D_B[a]	S_E[b]
Run 1	860	0.6	1.848	0.004
Run 3	915	0.6	1.782	0.008
Run 4*	970	0.6	2.000	0.000
Run 5	970	1.1	1.846	0.003
Run 6	970	1.6	1.827	0.005
Run 7	970	2.1	1.803	0.003
Run 8	970	2.6	1.800	0.005

[a] The fractal dimension of melt phase by the box-counting method

[b] S_E= standard error

*The D_B of the residual melt in Run 4 is Euclidean dimension and the D_B of the amphibole aggregation is 1.816 ±0.008.

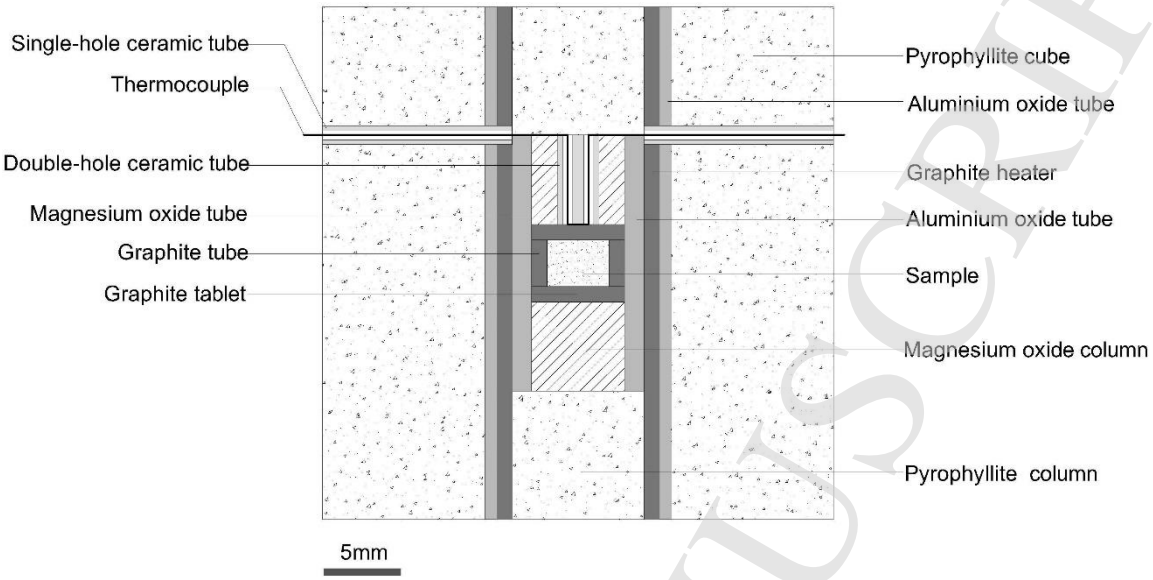

Fig. 1 Schematic cross-section of the sample assembly.

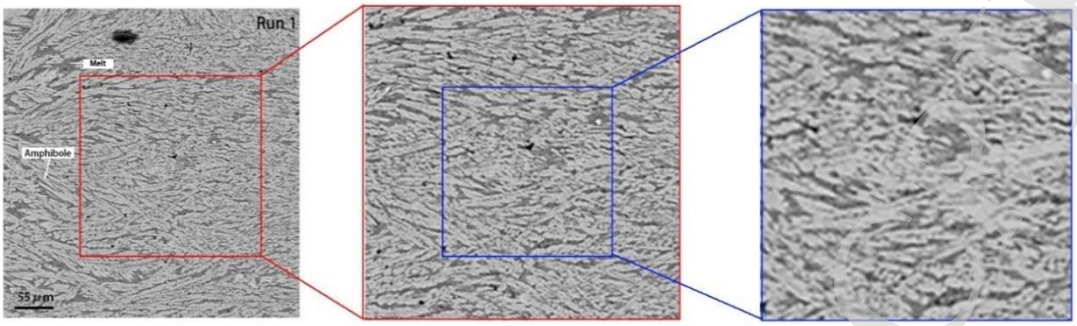

Fig. 2 The backscatter electron (BSE) image of amphibole grains and residual melt in Run 1 with different magnification showing the self-similarity.

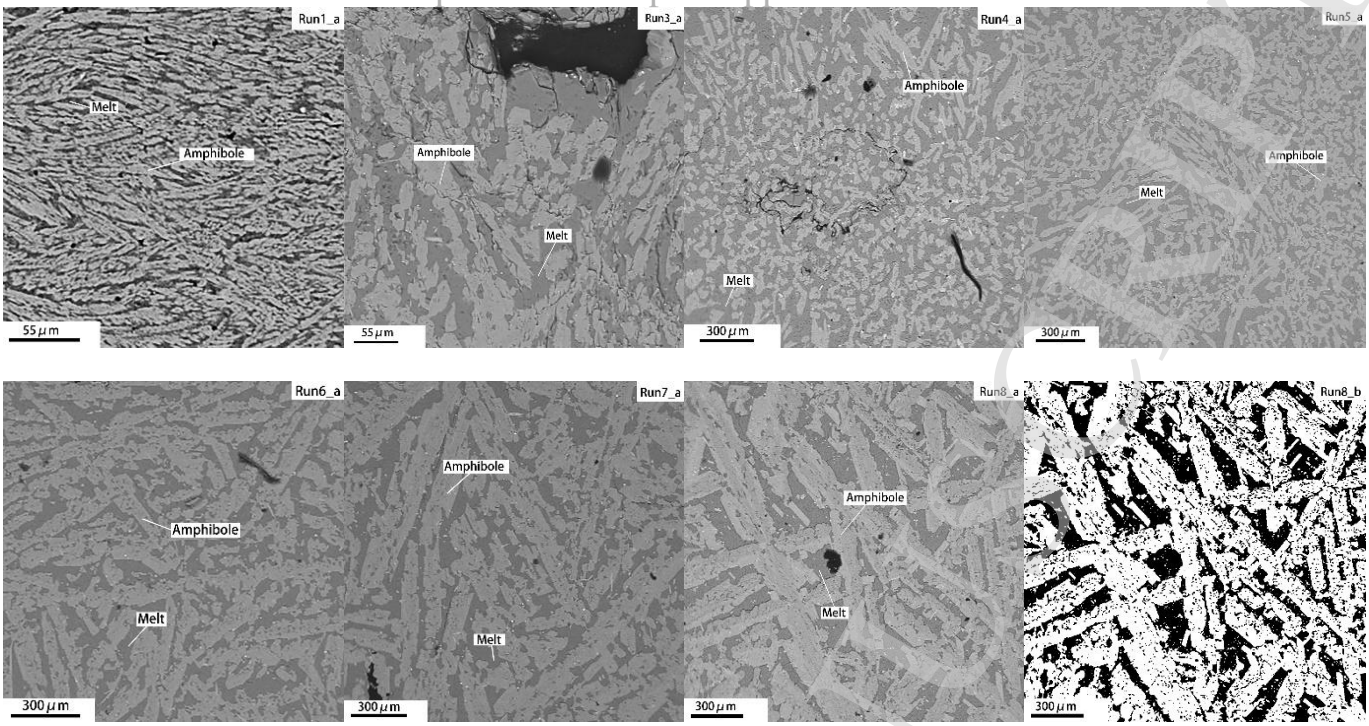

Fig. 3 The backscatter electron (BSE) images of the experimental products(a). An example of the binary image from Run 8_a with the amphibole phase shown in white and the residual melt phase in black (b).

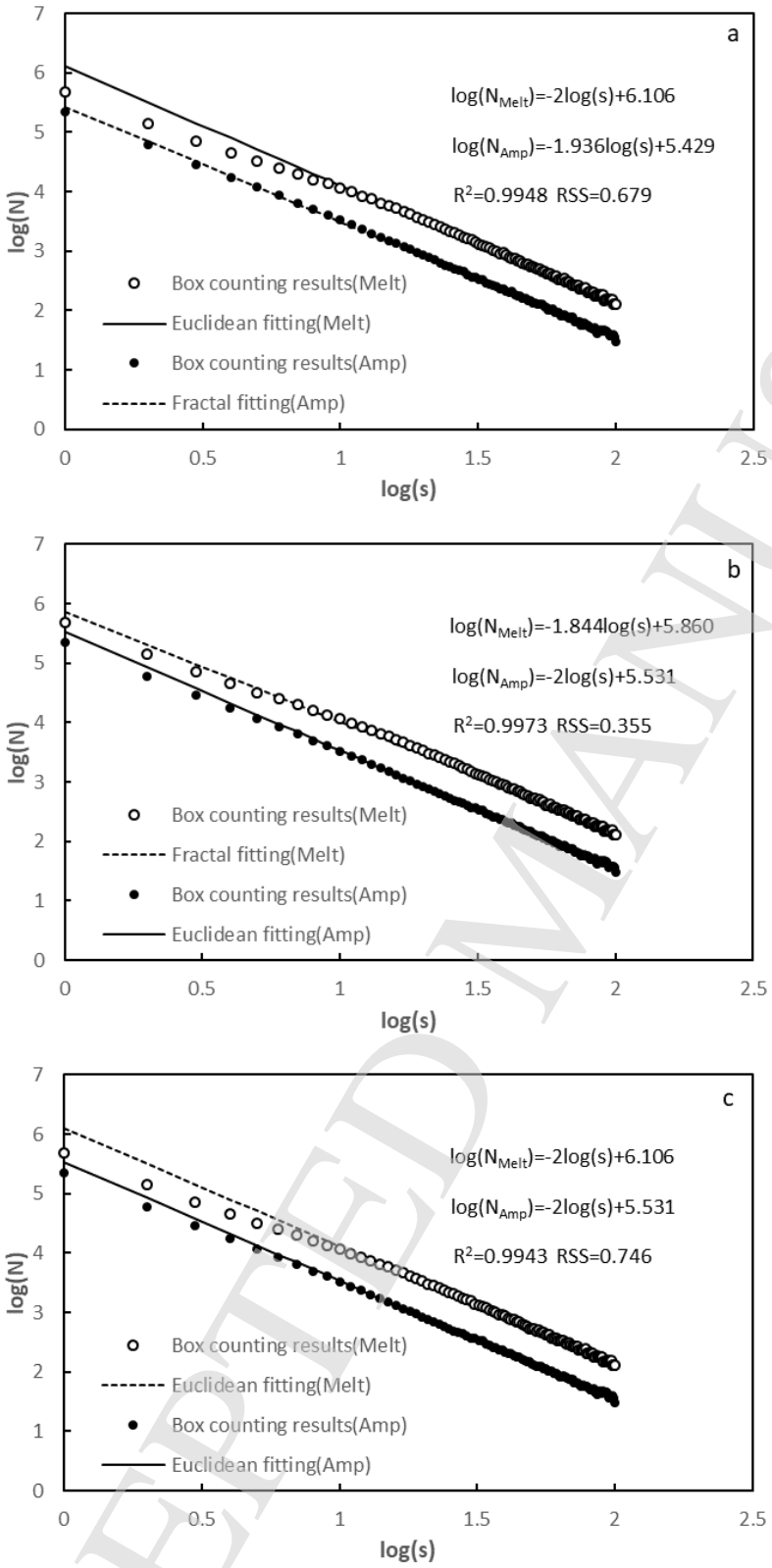

Fig. 4 Results of bi-phase box counting analyses performed on Run 1 image (Fig. 3b and 3c) with: (a) the Amp phase assumed to be fractal and the residual Melt phase Euclidean, (b) the Amp phase assumed to be Euclidean and the residual Melt phase fractal, and (c) both phases assumed to be Euclidean.

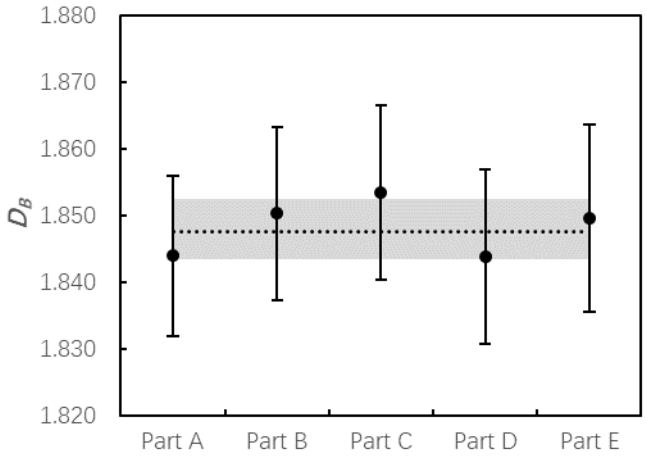

Fig. 5 The relation between fractal dimension D_B and different field of view (Part A, B, C, D and E) of Run 1 used for the fractal analyses. The dashed line shows the mean value (1.848) of all the different observations and the gray area represents standard deviation (±0.004) of the mean value.

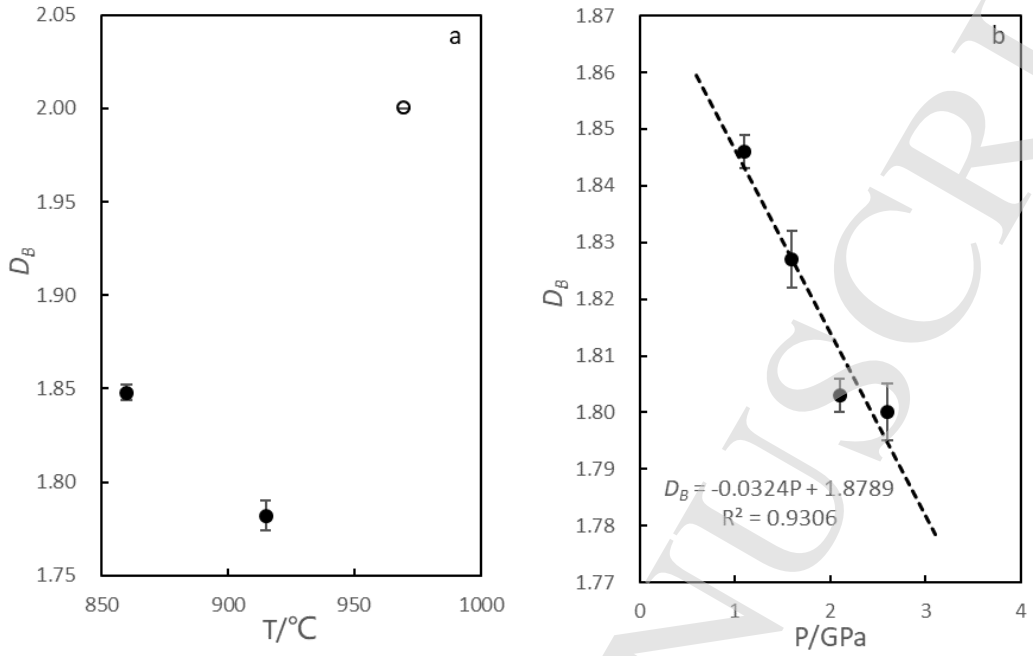

Fig. 6 The relation between fractal dimension D_B of the residual melt and temperature at 0.6 GPa (a). The relation between fractal dimension of the residual melt and pressure in the isothermal sequence (b). It should be note that the D_B of residual melt in Run 4 is the Euclidean dimension where the hollow dot is used to show difference from others (solid dots). The error bar of each data point represents the one-sigma error and the dashed line is the linear fitting of the data.